66. Han, S., Ching, Y.-C. & Rousseau, D. L. *Biochemistry* **29,** 1380–1384 (1990).
67. Morgan, J. E. & Wikström, M. *Biochemistry* **30,** 948–958 (1991).
68. Oliveberg, M., Hallén, S. & Nilsson, T. *Biochemistry* **30,** 436–440 (1991).
69. Poulos, T. L. *Adv. Inorg. Biochem.* **7,** 1–52 (1987).
70. Tabushi, I. *Coord. Chem. Revs.* **86,** 1–42 (1988).
71. Traylor, T. G. *Pure appl. Chem.* **63,** 265–274 (1991).
72. Babcock, G. T. in *Biological Applications of Resonance Raman Spectroscopy* Vol. 3 (ed. Sprio, T. G.) 294–346 (Wiley, New York, 1988).
73. Ogura, T., Takahashi, S., Shinzawa-Itoh, K., Yoshikawa, S. & Kitagawa, T. *Bull. Chem. Soc. Jpn.* (in the press).
74. Varotsis, C., Zhang, Y. & Babcock, G. T. *Proc. natn. Acad. Sci. U.S.A.* (submitted).
75. Ahmad, S. *et al. Inorg. Chem.* **27,** 2230–2233 (1988).
76. Proniewicz, L. M., Paeng, I. R. & Nakamoto, K. *J. Am. Chem. Soc.* **113,** 3294–3303 (1991).
77. Yoshikawa, S. & Caughey, W. S. *J. biol. Chem.* **265,** 7945–7958 (1990).
78. Blair, D. F., Witt, S. N. & Chan, S. I. *J. Am. chem. Soc.* **107,** 7389–7399 (1985).
79. Hansson, O., Karlsson, B., Aasa, R., Vänngård, T. & Malmström, B. G. *EMBO J.* **1,** 1295–1297 (1982).
80. Ogura, T., Takahashi, S., Shinzawa-Itoh, K., Yoshikawa, S. & Kitagawa, T. *J. biol. Chem.* **265,** 14721–14723 (1990).
81. Han, S., Ching, Y.-C. & Rousseau, D. L. *Nature* **348,** 89–90 (1990).
82. Wrigglesworth, J. M. *Biochem. J.* **217,** 715–719 (1984).
83. Vygodina, T. & Konstantinov, A. A. *Biochem. biophys. Acta* **973,** 390–398 (1989).
84. Vygodina, T. V., Schmidmeyer, K. & Konstantinov, A. A. *Biol. Membr.* (in Russian) (in the press).
85. Williams, R. J. P. *J. theor. Biol.* **1,** 1–17 (1961).
86. Mitchell, P. in *Of Oxygen, Fuels and Living Matter* (ed. Semenza, G.) 1–160 (Wiley, New York, 1981).
87. Chan, S. I. & Li, P. M. *Biochemistry* **29,** 1–12 (1990).
88. Nicholls, P. & Wrigglesworth, J. M. *Ann. N.Y. Acad. Sci.* **550,** 59–67 (1988).
89. Kobayashi, K., Une, H. & Hayashi, K. *J. biol. Chem.* **264,** 7976–7980 (1989).
90. Hill, B. C. *J. biol. Chem.* **266,** 2219–2226 (1991).
91. Antalis, T. M. & Palmer, G. *J. biol. Chem.* **257,** 6194–6206 (1982).
92. Wikström, M. & Krab, K. *Biochim. biophys. Acta* **549,** 177–222 (1979).
93. Blair, D. F., Gelles, J. & Chan, S. I. *Biophys. J.* **50,** 713–733 (1986).
94. Krab, K. & Wikström, M. *Biochim. biophys. Acta* **895,** 25–39 (1987).
95. Malmström, B. G. *FEBS Lett.* **250,** 9–21 (1989).
96. Scott, R. A. *A. Rev. Biophys. biophys. Chem.* **18,** 137–158 (1989).
97. Henderson, R. *et al. J. molec. Biol.* **213,** 899–929 (1990).
98. Wikström, M. & Krab, K. in *Energy Conservation in Biological Membranes* (eds Schäfer, G. & Klingenberg, M.) 128–139 (Springer, Berlin and Heidelberg, 1978).
99. Mitchell, P. *Ann. N.Y. Acad. Sci.* **550,** 185–198 (1988).
100. Williams, R. J. P. *FEBS Lett.* **226,** 1–7 (1987).

ACKNOWLEDGEMENTS. We thank T. Haltia, J. E. Morgan and C. Varotsis for discussion, and E. Schmidt and H. Vuorenmaa for help with the figures. Supported by the US National Institutes of Health (G.T.B.) and the Sigrid Jusélius Foundation (M.W.).

ARTICLES

Anisotropy of the inner core from differential travel times of the phases PKP and PKIKP

Kenneth C. Creager

Geophysics Program, University of Washington, Seattle, Washington 98195, USA

The difference between the travel times of compressional waves that turn in the Earth's liquid outer core (PKP-BC) and those that run in the solid inner core (PKIKP-DF) is primarily sensitive to structure near the inner-core boundary. Such differential travel times measured from short-period waveforms are consistent with small-amplitude deviations from radial symmetry except when ray paths are nearly parallel to the Earth's spin axis. These near-axial paths consistently produce large travel-time anomalies, providing compelling evidence for large-amplitude, axisymmetric anisotropy in the outermost portions of the inner core.

THE eigenfrequencies of the Earth's normal modes that are sensitive to seismic velocity structure at and below the core–mantle boundary are split much more than expected from the Earth's rotation and ellipticity. This anomalous splitting was first measured by Masters and Gilbert[1] and has since been thoroughly analysed[2–8]. There is general agreement on the measurements themselves, and on the inference that the structure causing the splitting is symmetric with respect to the Earth's spin axis (axisymmetric) and is at or below the core–mantle boundary. Two classes of models have been proposed to explain these observations. One is aspherical seismic-velocity structure dominated by the zonal spherical harmonic of degree 2 within the outer core, which is fast at the poles[2,3]. The second is axisymmetric anisotropy of the inner core with the fast direction parallel to the Earth's spin axis[4–7].

The travel-time residuals of rays turning in the inner core (PKIKP or P'_{DF}) reported by the International Seismological center (ISC) also show a strong axisymmetric pattern which was interpreted by Poupinet *et al.*[9] as zonal, degree-2 topography of the inner core, and by Morelli *et al.*[10] and Shearer *et al.*[11] as inner-core anisotropy. There is some uncertainty, however, in the interpretation of absolute travel times, owing to potential bias from earthquake mislocation and unknown aspherical structure of the crust, mantle and core–mantle boundary. Shearer and Toy[12] recognized that, in principle, the structure of the inner core can be resolved by analysing differential travel times of hand-picked PKP-BC (P'_{BC}) and P'_{DF} phases. The paths for these two rays remain within 300 km of each other throughout the mantle, but the DF phase enters the inner core whereas BC turns near the base of the outer core (Fig. 1), so differential travel-time residuals are most plausibly explained by structure either in a boundary layer at the base of the outer core, or structure in the inner core.

Like Shearer and Toy[12], I have picked differential times of P'_{BC} minus P'_{DF} from short-period recordings of the Global Digital Seismograph Network (GDSN). Among the common seismograms, our results are nearly identical, and show small, but geographically consistent, residuals with a root-mean square of 0.4 s. But to resolve axisymmetric inner-core anisotropy one needs observations of rays at a range of directions through the inner core relative to the Earth's spin axis. Whereas Shearer and Toy[12] analysed only one seismogram corresponding to a ray direction within 40° of this axis, I analyse 20 and find that

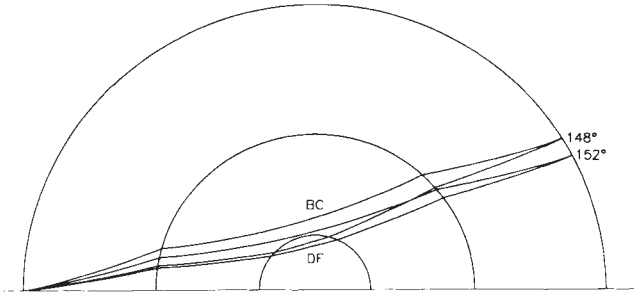

FIG. 1 Ray paths of P'_{DF} entering the solid inner core and P'_{BC} turning in the liquid outer core from a surface-focus earthquake to stations at epicentral distances of 148° and 152°.

TABLE 1 Models of inner-core anisotropy

Model	B (km s^{-1})	C (km s^{-1})	δv* (%)	Data	Phase	Distance range	Ref.
1			3.5†	IDA	modes		4
2			0.8–1.2‡	IDA	modes		7
3	−0.350	0.700	0.0–3.2§	ISC	DF	$170° < \Delta < 180°$	10
4			1.0	ISC	DF	$170° < \Delta < 180°$	10
5	−0.092	0.200	1.0	ISC	DF	$120° < \Delta < 140°, 154° < \Delta < 180°$	11
6	0.012	0.056	0.6	ISC	BC–DF	$145° < \Delta < 155°$	12
7	−0.165	0.557	3.5	GDSN	BC–DF	$146 < \Delta < 160°$	this work

* Polar velocity minus equatorial velocity, divided by equatorial velocity.
† Calculated equatorial PKIKP travel time minus polar time, divided by equatorial time, for rays straight through the inner core.
‡ Calculated equatorial PKIKP travel time minus polar time, divided by equatorial time, for rays turning at all depths in the inner core.
§ δv varies as $(r/R_{IC})^2$, where R_{IC} is the inner-core radius.

18 of them have large positive residuals in the range +2 to +4 s; these are 5 to 11 standard deviations away from the normal population of 244 observations whose ray angle with respect to the Earth's spin axis exceeds 40°. Because of their dependence on ray direction, and not on geographical sampling location, these new observations are most plausibly explained by anisotropy. The ray-path sampling of the differential times allows us to infer that the anomalous structure is at the base of the outer core, or at the top of the inner core. Finally, the sign of the anomalous travel-time residuals is consistent with the sign of the anomalous eigenfrequency splitting if the structure is assumed to be in the inner core, but has the opposite sign for an explanation in terms of structure at the base of the outer core. This study supports previous models of inner-core anisotropy except that, owing to the new observations, the amplitude of inner-core anisotropy is about three times larger than inferred from most previous body-wave estimates.

The amplitude ratios (BC/DF) of the 18 anomalous seismograms are also anomalous, with DF being consistently three times smaller than normal. The very small amplitudes of DF may explain why Shearer and Toy analysed only one of these anomalous seismograms, and may contribute to a systematic bias in the ISC Bulletin times, leading other researchers to underestimate the size of anisotropy in the inner core.

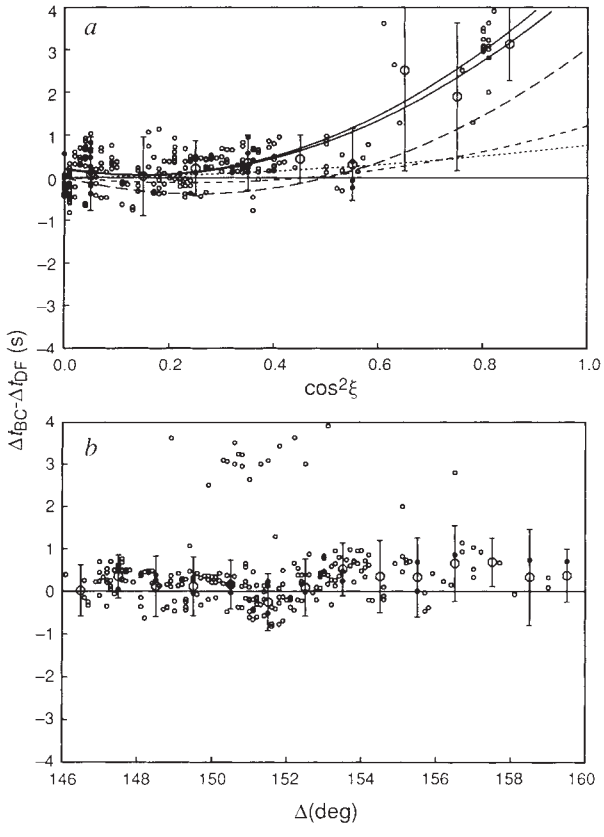

FIG. 2 Hand-picked differential travel-time residuals ($P'_{BC} - P'_{DF}$) plotted with respect to $\cos^2 \xi$ (*a*) and epicentral distance (*b*). ξ is the angle between the Earth's spin axis and the inner-core leg of the ray path. Bars show mean and two standard deviations of data binned at (*a*) 0.1 and (*b*) 1.0° intervals. Statistics in lower diagram are calculated using only times with $\cos^2 \xi < 0.6$. In *a*, differential travel times are calculated for surface-focus events at an epicentral distance of 150° using the anisotropy models of refs 10 (long-dashed line), 11 (short-dashed line) and 12 (dotted line) and that developed here (lower solid line). The latter model is also calculated for an epicentral distance of 152° (upper solid line). Models 3, 5, 6 and 7 of Table 1 are displayed.

Travel-time and amplitude observations

I extracted 2,500 short- and intermediate-period seismograms of P'_{BC} and P'_{DF} recorded in the epicentral distance range 146° to 160° on the GDSN from 1980 to 1986. These data were distributed by the National Earthquake Information Center. Of these seismograms 264 produce very clear arrivals of both P'_{BC} and P'_{DF}. Seismograms in which depth phases may have interfered with the later phase (P'_{BC}) were discarded. The waveform shapes of P'_{BC} and P'_{DF} are typically very similar, although the amplitude ratio P'_{BC}/P'_{DF} varies from 0.5 to 30.0, and P'_{DF} is typically, but not always, relatively depleted in high frequencies. Differential travel times were measured from the corresponding peaks and troughs of the two phases. These times were then averaged with weight given to the first cycle of each arrival. Because I only analysed the best data, and was able to match the shape of the two waveforms, the observed differential times are rarely, if ever, off by one or more cycles. Dominant periods are typically ~1 s. About 5% of the observations have very clear impulsive arrivals for both phases, but BC is dominated by high frequencies, whereas the high frequencies in DF are strongly attenuated. In these cases the differential times correspond to the difference between first arrivals. Only 13 of the times were read from intermediate-period records, and in every case the times are consistent with short-period records in similar geographical source–receiver geometries.

Differential travel-time residuals were calculated with respect to isotropic PREM[13] at a period of 1 s, using the earthquake locations given by the National Earthquake Information Center. Times were corrected for ellipticity[14]. Beyond 152°, the BC branch diffracts around the inner core. Travel times for diffracted waves are calculated by linear extrapolation of the curve of travel time against distance for BC turning rays. Positive residuals represent early DF or late BC, and correspond to fast velocities in the inner core of slow velocities at the base of the outer core.

Epicentre mislocations of 20 km and depth mislocations of 100 km cause errors in the differential times ranging from 0.15 to 0.30 s depending on the depth and epicentral distance. Subduction-zone earthquakes can be systematically mislocated by

20 km or more[15,16], causing systematic errors which would appear as geographically consistent signals of a few tenths of a second, but would rarely cause errors in excess of 0.5 s.

The histogram of differential travel-time anomalies has a remarkable distribution. Most of the times (92%) have a near-gaussian distribution with a mean of 0.2 s and a standard deviation of 0.4 s. The remaining 8% are clustered with a mean of 2.9 s, a full seven standard deviations away from the majority of the observations. The anomalous arrivals occur over a broad range of epicentral distances (Fig. 2*b*), event depths from 0 to 170 km and event magnitudes from 5.5 to 6.3, but the plot of residuals against the angle ξ between the Earth's spin axis and the ray path through the inner core cleanly separates all the anomalous phases from the normal phases (Fig. 2*a*).

Figure 3 shows six examples of anomalous arrivals. Some of my differential travel-time measurements could be in error by a few tenths of a second, but the very early P'_{DF} arrivals are unmistakable. Note also that the BC/DF amplitude ratios vary from 10 to 20. The amplitude ratios for the 'normal' observations in the same epicentral distance range cluster around 5. The BC/DF amplitude ratios for all paths with $\cos^2 \xi > 0.7$ are consistently three times larger than for paths to the same epicentral distances, but with $\cos^2 \xi < 0.6$. The small amplitude of the DF phase for large values of $\cos^2 \xi$ makes the observations of 'anomalous' phases difficult to obtain because DF is seldom above the noise level.

Anisotropy or heterogeneity?

The cause of these anomalous observations can best be discerned by analysing the ray-path sampling of the Earth's interior. Figure 4 shows the observed anomalies, plotted in map view at the turning points, the inner-core boundary intersection points of DF, and the source and receiver points. The turning-point plot shows remarkable coherence, even though the r.m.s. signal in the 'normal' observations is only 0.4 s. This consistency suggests that the r.m.s. reading error is much less than 0.4 s, perhaps as small as 0.2 s. The anomalous times (large plus signs) are widely distributed. There are 14 under Columbia, and one under each of western China, the Philippines, the south central Pacific and the central Atlantic. With the exception of the 'anomalous' phases, the times are dominated by negative residuals in the western hemisphere and positive in the eastern hemisphere. These small, but consistent, residuals are plausibly explained by large-scale aspherical structure (perhaps degree 1) of the inner core, or the base of the outer core, with small (<0.5%) velocity contrast. Alternatively, they may be caused by systematic biases in earthquake mislocations.

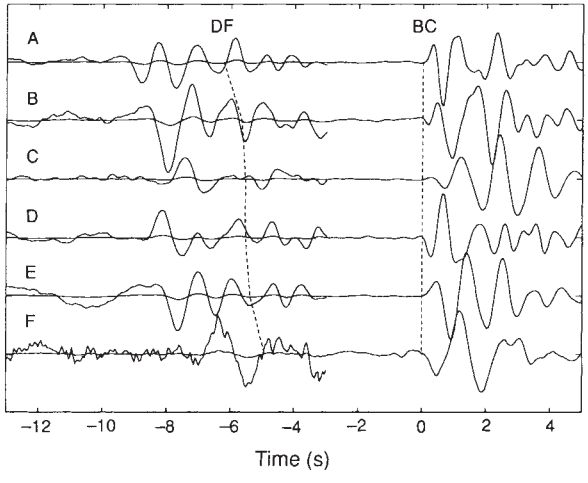

FIG. 3 Six vertical-component, short-period seismograms aligned on the P'_{BC} arrival (time = 0). Dashed lines indicate the differential travel times predicted by Earth model PREM. From −13 to −3 s each seismogram is displayed twice, once at the same scale as the BC phase, and once magnified by a factor of 10 so that the DF phase can be seen. For these anomalous paths ($\cos^2 \xi \approx 0.8$) the BC − DF differential time is, on average, 3 s greater than predicted by PREM. Seismograms A–E are recorded at station COL (Alaska) from earthquakes under the South Sandwich Islands which are separated by as much as 130 km in epicentre and vary in depth from 30 to 170 km. F is recorded at RSNT (Canada) from an earthquake under the Atlantic–Indian Rise.

The other two diagrams of Fig. 4 are more complicated and internally less consistent. In particular, it is worth noting that in the plots of both turning points and inner-core intersection points, the western hemisphere mostly contains negative residuals, except for the 'anomalous' (plus) times, most of which are also in this hemisphere. Geographically, the anomalous phases are widely distributed and interspersed with the normal observations, suggesting that they cannot be explained by a model of large-scale isotropic heterogeneity.

Alternatively, we can check whether the observations are consistent with simple models of anisotropy. Figure 5*a* displays the differential time residuals in an equal-area, azimuthal projection of the P'_{DF} ray direction in the inner core. The centre of the diagram corresponds to rays travelling parallel to the spin axis, and the perimeter represent rays in the equatorial plane. This diagram separates the anomalous observations from the normal ones. It also separates the normal observations into groups with considerable internal consistency.

Following refs 10–12, I consider simple models of anisotropy. Let us consider uniform anisotropy of the inner core with cylindrical symmetry about the Earth's spin axis. For weak anisotropy, the compressional wave speed can be approximated[12] by $\delta v_p(\xi) = A' + B' \cos 2\xi + C' \cos 4\xi$ or equivalently by[10] $\delta v_p(\xi) = V_{eq}(1 + \varepsilon \cos^2 \xi + \sigma \cos^2 \xi \sin^2 \xi)$ where ξ is the angle between the spin axis and the P'_{DF} ray segment through the inner core. For the PREM velocity model, rays through the inner core follow circular paths whose radii of curvature are so large that a ray changes direction by less than 1° during transit through the inner core. To a good approximation, each ray can be characterized by a constant angle ξ. The above equations can be rewritten in a third equivalent form as a parabola in $\cos^2 \xi$:

$$\delta v_p(\cos^2 \xi) = A + B \cos^2 \xi + C (\cos^2 \xi)^2 \qquad (1)$$

using the conversion equations $A = A' - B' + C' = V_{eq}$, $B = 2B' - 8C' = V_{eq}(\varepsilon + \sigma)$, $C = 8C' = -V_{eq}\sigma$. Using this parameterization, and considering δv_p to be anomalies with respect to PREM, I have inverted the hand-picked differential travel times using least squares and obtain $A = 0.018$ km s^{-1}, $B = -0.165$ km s^{-1}, and $C = 0.557$ km s^{-1}. The wave speed in the polar direction is 3.5% faster than in the equatorial direction.

This simple two-parameter model explains 69% of the variance in the 264 observations. To examine whether the data require an axisymmetric structure, I consider cylindrically symmetric anisotropy, but vary the direction of the symmetry axis. For each axis, I invert for the best model parameters and calculate the variance reduction (Fig. 5*b*). The best fit is achieved when the symmetry axis is 5° from the spin axis at 85° S, 300° E, but acceptable models (variance reductions of 50% or more) are achieved for models in which the symmetry axis is displaced up to 5° from the South Pole along a longitude of 180° and 35° along the 0° longitude (Fig. 5*b*). It is clear from the ray-angle diagram (Fig. 5*a*) that more observations with ray angles near the spin axis will help constrain the models, especially observations with longitudes near 270°.

Comparison with previous models

Table 1 summarizes models of inner-core anisotropy. Models 3–7 are parameterized in the same way as above (equation (1)), except that the amplitude of the anisotropy in model 3 varies as r^2, whereas models 4–7 assume uniform anisotropy. Theoretical travel-time anomalies depend only on ξ, on epicentral distance (Δ) and weakly on hypocentral depth. Because the ray paths are nearly straight, and the inner-core velocity varies

slowly with depth, the theoretical time residuals can be approximated by

$$\delta t^{DF}(\Delta, \cos^2 \xi) \approx (-T(\Delta)/V)\delta v_p(\cos^2 \xi) \quad (2)$$

where $T(\Delta)$ is the travel time through the inner core and $V = 11\ km\ s^{-1}$ is the velocity near the top of inner core. Using this scaling, I compare the actual observations with the travel times predicted at $\Delta = 150°$ ($T = 124$ s) for models 3, 5, 6 and 7 (Fig. 2*a*). The solid lines show the weak dependence on Δ by displaying predicted times for $\Delta = 150$ and 152°, the distance range of the bulk of our 'anomalous' observations (Fig. 2*b*). Model 3 is corrected for the r^2 dependence by multiplying the right-hand side of equation (2) by $1/3 + 2/3(r_t/R_{IC})^2$ where r_t is the turning radius of the ray and R_{IC} is the radius of the inner core. For $\Delta = 150°$, this factor is 0.77.

All seven models are consistent with the fast direction being parallel to the spin axis, but there is considerable variation in the amplitude of the anisotropy. Morelli *et al.*[10] proposed two models of anisotropy consistent with absolute P'_{DF} times from the ISC in the epicentral distance range 170 to 180°. These rays propagate nearly straight through the centre of the inner core and thus sample nearly all depths of the inner core. Their data could be explained by anisotropy decaying as r^2 with 3.2% contrast at the surface of the inner core (model 3), or by uniform anisotropy with a 1% contrast (model 4). An analysis of absolute P'_{DF} times from the ISC in the epicentral distance ranges 120–140° and 154–180°, which correspond to rays turning within 70 km of the inner-core boundary and more than 310 km below this boundary, respectively, is consistent with 1% uniform anisotropy (model 5)[11]. Anomalous times reported here occur in an intermediate distance range (148–156°, Fig. 2*b*), but the apparent anisotropy is 3–4 times larger in amplitude.

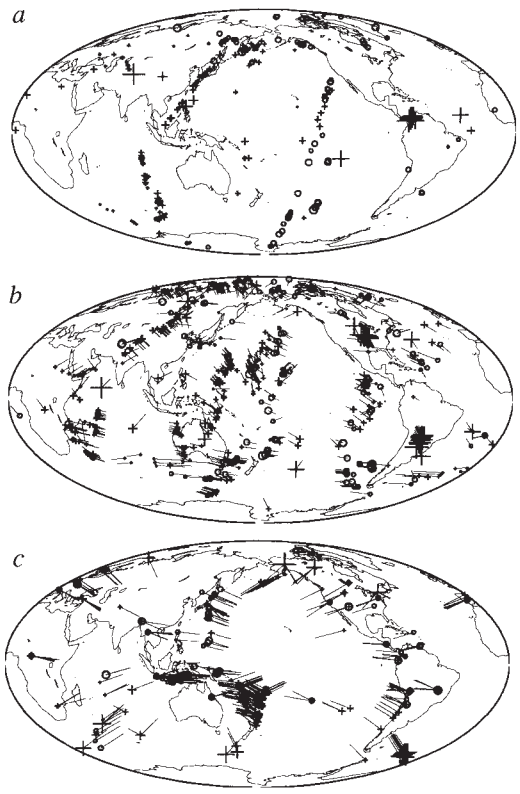

FIG. 4 Differential travel-time residuals ($P'_{BC} - P'_{DF}$) plotted as a function of (*a*) ray turning point (*b*) inner-core intersection points and (*c*) source and receiver locations. +, positive; ○, negative. Residual magnitude is proportional to symbol size with the largest symbols representing a 4-s residual. In the two lower panels each observation corresponds to two geographical positions; line segments point towards the other position of the pair. The anomalous times, interpreted here as being caused by anisotropy, are the large plus symbols. In the upper diagram, there are 14 under Columbia, and one under each of western China, the Philippines, the south central Pacific and the central Atlantic.

The waveform data set analysed here is similar to that of Shearer and Toy[12], and the observed times are nearly identical (compare Fig. 4*a* with their Fig. 6) except that they measured only one time with $\cos^2 \xi > 0.6$. Their model matches both their observations and the subset of mine with $\cos^2 \xi < 0.6$, but is not consistent with my observations for $\cos^2 \xi > 0.6$ (Fig. 2*a*). Shearer and Toy[12] also analysed arrival times reported in the ISC Bulletin. They discarded differential times (BC − DF) with residuals in excess of 1.5 s, apparently because the scatter in these times is small (see their Fig. 11) and their hand-picked residuals never exceeded ±1 s. They found that weak (0.6%) anisotropy is consistent with both the ISC and GDSN observations. I have analysed the ISC data in the epicentral distance range 150–156°, but with a residual cut-off of 3.5 s. There are 95 observations with $\cos^2 \xi > 0.6$, 53 of which corresponded to paths from 25 earthquakes in the South Sandwich Islands to nine stations in Alaska. The geographical positions of sources and receivers are similar to those for seismograms A–E (Fig. 3). The mean (±1 s.d.) for these 53 observations is 2.6 ± 0.8 s, consistent with the anomalous times measured here and consistent with 3% anisotropy. These times were rejected, however, by Shearer and Toy[12]. No other geographical region is as well sampled, and all other regions show much less internal consistency. The mean residual of the remaining 42 times having $\cos^2 \xi > 0.6$ is 0.5 s. These small residuals are inconsistent with the anisotropy model presented here.

For comparison with body-wave models, I estimate δv (defined in Table 1) from mode-derived models as the theoretical PKIKP travel-time difference between pole-perpendicular and pole-parallel paths divided by the time of the pole-perpendicular paths. On the basis of modal data, Woodhouse *et al.*[4] constructed model 1 with $\delta v > 3\%$ for rays through the centre of the Earth, whereas Li *et al.*[7] produced model 2 with δv varying from 0.8 to 1.2% for different ray turning depths (estimated from their Fig. 13). The latter model is consistent with PKIKP travel times predicted by body-wave models 4–6. The argument consistently delivered in refs 4–7 is that there exists a model of axisymmetric anisotropy of the inner core that is consistent with the mode data, but that these data cannot uniquely determine inner-core anisotropy. Given the variety of published models that are consistent with the modes, it would seem that there exists a model of axisymmetric inner-core anisotropy of the form analysed by Li *et al.*[7] that is consistent both with the modes and with the travel times presented here. Note, however, that the interpretation that mode splitting is primarily caused by inner-core anisotropy remains controversial. Observation of modes that had not previously been analysed, combined with an analysis of the radial distribution of elastic energy for these modes, has led Widmer[8] to conclude that the primary cause for anomalous splitting is structure above the inner core, but below the mantle.

The hand-picked times analysed here, and a re-evaluation of some of the ISC differential times, suggest that previous body-wave studies have underestimated the size of the inner-core anomaly by between 40% (model 3) and a factor of 3 or more (models 4–6). The difference results primarily from new waveform observations of highly anomalous differential times in the critical ray-sampling direction nearly parallel to the Earth's spin axis. Observations for this sampling direction in the ISC catalogue are rare, but show consistently anomalous times for South Sandwich Islands earthquakes to Alaska at an epicentral distance of ~150–154° (this work), and in the distance range 170–180° (ref. 7). Other geographical or epicentral distance ranges do not show as strong an anomaly in the ISC catalogue[11]. It is difficult to reconcile all these observations with a simple model of the inner core, although a model with large-amplitude

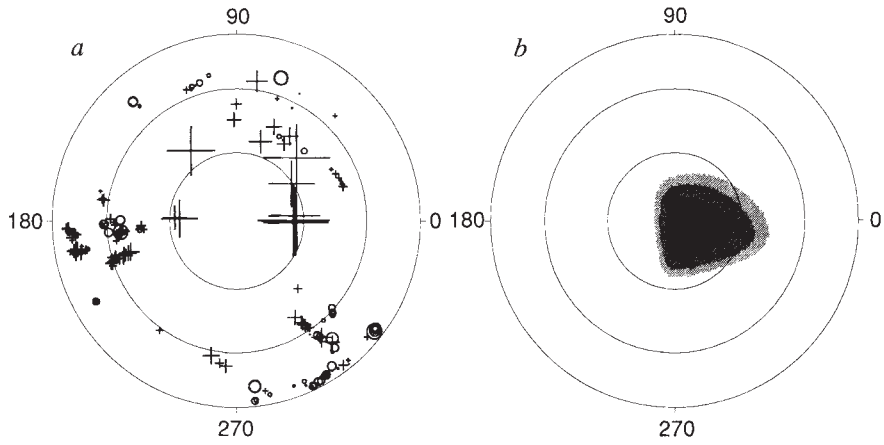

FIG. 5 *a*, Differential travel-time residuals as a function of inner-core P'_{DF} ray direction displayed on an equal-area, azimuthal projection of the Southern Hemisphere. Ray direction latitude is 90° S at the centre and 0° at the circumference, with latitudes of 0, 30 and 60° S shown by concentric circles. The longitude of the ray direction in the Southern Hemisphere is measured counterclockwise from the right of the diagram as if you were looking at the Earth down from the North Pole. *b*, Variance reduction plotted against direction of the symmetry axis of a uniformly anisotropic inner core with cylindrical symmetry. Black represents a variance reduction of >70% contour interval is 10%. White is less than 40%.

anisotropy in a layer extending from about 100 to 300 km depth in the inner core, and weak anisotropy outside, may go a long way towards explaining all the observations. Recall that the rays analysed here turn ~100–300 km beneath the inner-core boundary, whereas those analysed by Shearer *et al.*[11] turn either above or below this region. An alternative explanation, suggested by the observation made here that P'_{DF} rays with $\cos^2 \xi > 0.6$ have anomalously low amplitudes, is that these phases are systematically difficult to observe above ambient noise. This may lead to unreliable travel-time picks in the ISC Bulletin for this sampling direction. An analysis of differential times and amplitude ratios measured from digital waveforms of P'_{CD} minus P'_{DF} (ref. 17) in the distance range 130–140°, and P'_{AB} minus P'_{DF} in the distance range 146–180°, may help resolve the depth dependence of anisotropy.

Implications

My primary result is that 92% of the P'_{BC} minus P'_{DF} differential travel-time residuals are small (r.m.s. scatter of 0.4 s), whereas the mean of the remaining 8% of the times is 2.9 s, seven standard deviations away from the 'normal' observations. The geographical sampling of anomalous and normal paths overlaps (Fig. 4*a*), but all of the anomalous observations (early, small-amplitude DF) have inner-core ray paths nearly parallel to the Earth's spin axis. The observations can be explained (69% variance reduction of 264 independent observations) using a two-parameter model of uniform, cylindrically symmetric anisotropy. These data only sample the outer 300 km of the inner core, and the anomalous paths sample mainly latitudes within 45° of the Equator but are widely, although not uniformly, distributed in longitude. There is therefore a strong case for P-wave anisotropy at low latitudes in the outermost inner core which is 3.5% fast parallel to the Earth's spin axis. From differential times alone, we cannot distinguish between inner-core anisotropy advancing the times of DF or anisotropy in a boundary layer at the base of the outer core delaying the times of BC. Inner core anisotropy is, however, consistent with the absolute time observations of P'_{DF} (refs 10, 11), and with the sign of anomalous mode splitting, whereas the outer-core boundary layer hypothesis would produce mode splitting of opposite sign to the observations. In addition to anisotropy, there seems to be large-scale heterogeneity which is not dominantly axisymmetric (Fig. 4*a* and *b*) and is small in amplitude, giving rise to travel-time anomalies typically less than 0.5 s. This could be caused by structure in the inner core or a boundary layer at the base of the outer core.

The symmetry axis of models of cylindrically symmetric uniform anisotropy that best fits the observations is 5° from the Earth's spin axis, and the locus of all symmetry axes that provide reasonable fits (say >50% variance reduction) includes the spin axis, but only 6% of the range of possible directions (Fig. 5*b*). These observations constrain the symmetry axis to be so near to the rotation axis that their coincidence is unlikely to be due to random chance.

The inner core seems to be made primarily of the hexagonally close-packed ε phase of iron[18], whose compressional wave-speeds are anisotropic. The magnitude of anisotropy increases with pressure, but decreases with temperature, so its value extrapolated to inner-core conditions is highly uncertain. Two mechanisms for aligning the iron crystals are well organized large-scale convective flow and preferred alignment as the inner core freezes. If the temperature of the inner core is near the solidus, it may be convectively unstable[19]. The lowest mode of convection of a homogeneous sphere heated from within is characterized by flow straight through the centre with return flow along the entire surface[20]. If the axis of symmetry of this flow is the spin axis, one obtains nearly uniform simple shear at low latitudes which could align the iron crystals in a well organized manner[21]. This mechanism would not produce the mode of uniform anisotropy proposed here but the anisotropy would be roughly uniform in the region sampled by the anomalous paths, and produce a model that is consistent with the differential times. Alternatively, anisotropy could have been frozen in during inner-core formation and aligned relative to the spin axis (maximum moment of inertia). For the inner core to be aligned now this principal axis of inertia would have had to remain unchanged over the growth time of the outer 300 km of the inner core, perhaps as long as 10^9 years.

The amplitude ratios BC/DF of the anomalous phases are three times larger than the ratio measured for 'normal' paths at the same epicentral distances. This ratio commonly exceeds 15. The small-amplitude DF phases make travel-time picks of the anomalous phases rare and prone to error because DF is seldom above the noise. Because of its consistency and large magnitude, the amplitude observations may place strong constraints on core structure, which will be analysed elsewhere (T.J.M. and K.C.C., manuscript in preparation). Possible explanations are that high velocities in the inner core advance the times and cause anomalous geometrical spreading, reducing amplitudes. Alternatively, the transmission and reflection coefficients at the inner-core boundary may be strongly affected by the anisotropic properties of the inner core. Further analysis of waveforms of P'_{DF} along ray directions nearly parallel to the Earth's spin axis is needed to improve the resolution of inner-core structure.

Received 12 August 1991; accepted 3 March 1992.

1. Masters, G. & Gilbert, F. *Geophys Res. Lett.* **8**, 569–571 (1981).
2. Ritzwoller, M., Masters, G. & Gilbert, F. *J. geophys. Res.* **91**, 10203–10228 (1986).
3. Ritzwoller, M., Masters, G. & Gilbert, F. *J. geophys. Res.* **93**, 6369–6396 (1988).
4. Woodhouse, J. H., Giardini, D. & Li, X.-D. *Geophys. Res. Lett.* **13**, 1549–1552 (1986).
5. Giardini, D., Li, X.-D. & Woodhouse, J. H. *Nature* **325**, 405–411 (1987).
6. Giardini, D., Li, X.-D. & Woodhouse, J. H. *J. geophys. Res.* **93**, 13716–13742 (1988).
7. Li, C.-D., Giardini, D. & Woodhouse, J. H. *J. geophys. Res.* **96**, 551–577 (1991).

8. Widmer, R. thesis, Univ. of California, San Diego (1991).
9. Poupinet, G., Pillet, R. & Souriau, A. *Nature* **305,** 204–206 (1983).
10. Morelli, A., Dziewonski, A. M. & Woodhouse, J. H. *Geophys. Res. Lett.* **13,** 1545–1548 (1986).
11. Shearer, P. M. Toy, K. M. & Orcutt, J. A. *Nature* **333,** 228–232 (1988).
12. Shearer, P. M. & Toy, K. M. *J. geophys. Res.* **96,** 2233–2247 (1991).
13. Dziewonski, A. M. & Anderson, D. L. *Phys. Earth planet. Inter.* **25,** 297–356 (1981).
14. Dziewonski, A. M. & Gilbert, F. *Geophys. J. R. astr. Soc.* **44,** 7–17 (1976).
15. Kennett, B. L. N. & Engdahl, E. R. *Geophys. J. Int.* **105,** 429–465 (1991).
16. Boyd, T. M. & Creager, K. C. *J. geophys. Res.* **96,** 2267–2291 (1991).
17. Cormier, V. F. & Choy, G. L. *Geophys. Res. Lett.* **13,** 1553–1556 (1986).
18. Brown, J. M. & McQueen, R. G. *J. geophys. Res.* **91,** 7485–7494 (1986).
19. Jeanloz, R. & Wenk, H. R. *Geophys. Res. Lett.* **15,** 72–75 (1988).
20. Chandrasekhar, S., *Hydrodynamic and Hydromagnetic Stability* (Clarendon, Oxford, 1961).
21. Wenk, H. R., Takeshita, T., Jeanloz, R. & Johnson, G. C. *Geophys. Res. Lett.* **15,** 76–79 (1988).

ACKNOWLEDGEMENTS. I thank P. M. Shearer for preprints, code to read GDSN data from CD-ROMs and a review and R. T. Merrill and J. M. Brown for discussions. The digital seismic data came primarily from the GDSN operated by the US Geological Survey. This work was supported by the NSF.

Lymphoproliferation disorder in mice explained by defects in Fas antigen that mediates apoptosis

Rie Watanabe-Fukunaga*, Camilynn I. Brannan†, Neal G. Copeland†, Nancy A. Jenkins† & Shigekazu Nagata*‡

* Osaka Bioscience Institute, 6-2-4 Furuedai, Suita-shi, Osaka 565, Japan
† Mammalian Genetics Laboratory, ABL-Basic Research Program, NCI–Frederick Cancer Research and Development Center, Frederick, Maryland 21702, USA

Fas antigen is a cell-surface protein that mediates apoptosis. It is expressed in various tissues including the thymus and has structural homology with a number of cell-surface receptors, including tumour necrosis factor receptor and nerve growth factor receptor. Mice carrying the lymphoproliferation (*lpr*) mutation have defects in the Fas antigen gene. The *lpr* mice develop lymphadenopathy and suffer from a systemic lupus erythematosus-like autoimmune disease, indicating an important role for Fas antigen in the negative selection of autoreactive T cells in the thymus.

T-CELL precursors arise in the bone marrow and then mature in the thymus after interaction with the thymic microenvironment[1]. During maturation, T cells recognizing self-antigens are destroyed by a process called apoptosis, whereas others are positively selected[2,3]. The lymphoproliferation mutation (*lpr*) seems to interfere with T-cell maturation. The *lpr* is autosomal recessive and the phenotype includes formation of multiple autoantibodies and accumulation of large numbers of non-malignant $CD4^-CD8^-$ T lymphocytes in lymph nodes and the spleen[4]. Two independent spontaneous *lpr* mutations have been identified, *lpr* and lpr^{cg}. The original *lpr* mutation occurred during the derivation of the MRL/MpJ strain[5] and has been transferred onto a number of other inbred strain backgrounds, including C3H and C57BL[6]. The other mutation is lpr^{cg} in the CBA/K1Jms mouse strain[7]. The clinical syndrome of *lpr* and lpr^{cg} mice is characterized by hypergammaglobulinaemia, anti-DNA antibodies, rheumatoid factor, and circulating immune complexes as well as arthritis and glomerulonephritis, which resembles human systemic lupus erythematosus (SLE)[4]. Studies of *lpr* mice suggest that there is a defect in negative selection of self-reactive T lymphocytes in the thymus[8,9]. Excessive numbers of self-reactive T lymphocytes released into peripheral organs seem to be responsible for the autoimmune disease in *lpr* mice.

Here we provide evidence that *lpr* encodes the structural gene for the mouse Fas antigen[10]. A mouse monoclonal antibody has been prepared which has a cytolytic activity on human cells expressing the Fas antigen[11]. Cloning of Fas antigen complementary DNA from human[12] and mouse cells[10] indicates that the Fas antigen is a protein containing a single transmembrane domain with a calculated M_r of 35,000 (35 K) (refs 10, 12). Fas antigen from both species shows structural homology with a number of cell-surface receptors, including tumour necrosis factor (TNF) receptors and the low-affinity nerve growth factor receptor[10,12]. Northern analysis indicates the Fas antigen messenger RNA is expressed in a limited number of tissues, including the thymus, liver, ovary and heart[10]. When human Fas antigen is expressed in mouse cell lines, it can induce Fas antigen antibody-triggered cell death[12]. Characterization of the process of cell death indicates that Fas antigen mediates apoptosis[12]. Expression of Fas antigen in the thymus and its role in apoptosis provides an explanation for the phenotypes of *lpr* mice. These studies further suggest a role for the Fas antigen in the negative selection of autoreactive T cells in the thymus.

Expression of Fas mRNA in *lpr* mice

The mouse Fas antigen gene has been assigned to chromosome 19 by interspecific backcross analysis[10]. When our linkage map of mouse chromosome 19 was aligned with a composite linkage map (GBASE, Jackson Laboratory) we found that the Fas antigen locus mapped near *lpr*[13].

To determine whether the *lpr* mutation affects Fas antigen mRNA expression, northern analysis of wild-type and mutant *lpr* tissues was done using a mouse Fas antigen cDNA probe. Total cellular RNAs were isolated from two different strains carrying the *lpr* mutation (MRL *lpr*/*lpr* and C3H *lpr*/*lpr*) and their parental wild-type controls (MRL +/+ and C3H +/+). In agreement with previous observations[10], a 2.1 kilobase (kb) Fas antigen mRNA is detected in the liver and thymus of mice wild type at *lpr* (Fig. 1*a*). Almost no Fas mRNA is observed in homozygous *lpr* mice. Reprobing the same blot with human elongation factor-1α (EF-1α) cDNA[14] reveals a band of 2.2 kb in all RNA preparations (Fig. 1*b*). To confirm the absence of Fas mRNA in *lpr* mice, single-stranded cDNAs were synthesized from thymus RNA of wild-type and *lpr* mice and amplified by the polymerase chain reaction (PCR), using Fas antigen oligonucleotide primers. PCR amplification of RNA from wild-type mice gave a band of the expected size (420 bp), whereas no such band was amplified from *lpr* mice (Fig. 1*c*).

‡ To whom correspondence should be addressed.